Chapter

3D Point Cloud-Based Tree Canopy Visualization for a Smart Deployment of Mobile Communication Systems

Yunus Egi and Engin Eyceyurt

Abstract

Mobile communication is one of the most important parameters of smart cities in terms of maintaining connectivity and interaction between humans and smart systems. However, In the deployment process of Mobile Communication Systems (MCS), Radio Frequency (RF) engineers use location depended empirical Signal Strength Path Loss (SSPL) models ending up with poor signal strength and slow data connection. This is due to the fact that empirical propagation models usually are restrained by the environment and do not implement state of the art technologies, including Unmanned Aerial Vehicles (UAV), Light Detection and Ranging (LiDAR), Image Processing, and Machine Learning to increase efficiency. Terrains involving buildings, hills, trees, mountains, and human-made structures are considered irregular terrains by telecommunication engineers. Irregular terrains, specifically trees, significantly affect MCS's efficiency because of their complex pattern resulting in erroneous signal fading via multi-path reflection and absorption. Therefore, a virtual 3D environment is required to extract the required 3D terrain pattern and elevation data from the environment. Once this data is processed in the machine learning algorithm, an adaptive propagation model can be formed and can significantly improve SSPL prediction accuracy for MCS. This chapter presents 3D point cloud visualization via sensor fusion and 2D image color classification techniques, which lead to a novel propagation model for the smart deployment of MCS. The proposed system's main contribution is to develop an intelligent environment that eliminates limitations and minimizes related signal fading prediction errors. In addition, having better connectivity and efficiency will resolve the communication problem of smart cities. The chapter also provides a case study that significantly outperforms other empirical models with an accuracy of 95.4%.

Keywords: point cloud, image processing, direct geo-referencing, machine learning, radio networks, signal strength path loss

1. Introduction

In recent years, the number of the mobile subscriber has reached 5.11 billion worldwide with a 2% increase [1]. This is due to the fact that available technologies such as LTE and 5G are in use in smart cities to communicate and share the data

through video conferencing, online shopping, working from home, smart transportation and etc. In addition, Covid-19 lockdowns cause 70% increase in internet usage and 12% increase in streaming [2]. Accessibility of higher throughput transfers in uplink and downlink led to accelerating the digitization process of new technological advancements including Internet of Things (IoT), cloud computing, big data analysis, and machine learning [3]. The digitization process is crucial in terms of creating smart cities. As the usage of LTE and 5G technologies increases in smart cities, the low-cost broadcast systems designed for different terrains become more critical. Lands containing mountains, hills, vegetation, and human-made structures are considered irregular terrains in telecommunication due to their complex structure and surface pattern. However, vegetation has more impact on wireless communication since leaves and branches cause faster absorption of signal strength through multi-path reflection [4, 5]. Empirical propagation models such as Free space, Log-Normal (LN), and Cost-231 Hata models are limited by the environment selection which may lead to inaccurate results in SSPL predictions [6, 7]. In order to avoid faulty results, it is essential to take into account both the elevation and the terrain shapes in SSPL calculations. For instance, in **Figure 1**, ignoring the tree canopies falling into the Fresnel zone between the transmitter and the receiver affects the performance of the transmitted signal and causes false path loss estimation as the main signal has interference from the tree canopy. It is not possible to physically distinguish between vegetation and the rest of the surrounding environment in practical applications. When equipped with a geo-referenced satellite image and a corresponding geo-referenced 3D point cloud, it becomes possible to create virtual twin environment and extract the features of the environment to predict SSPL as seen in **Figure 2**. In airborne LiDAR, Geographical Mobile Mapping System (Geo-MMS), the GPS and IMU provide the exact location and orientation of airborne LiDAR [8]. The LIDAR sends laser pulses to objects on the earth and collects the reflected pulses from the environment. The distances are found by calculating the time delay (μ) between the transmitted and received laser pulses [9]. The obtained geo-referenced data points form a 3D point cloud that will give the surface's property, such as the height and width of the obstacles. However, since these features will not be sufficient to classify trees from the environment, 2D satellite imagery will be used. The 2D satellite image has a colorful and classifiable character. We can use this feature to extract trees from the 3D image by classifying them. This process is illustrated in **Figure 3**.

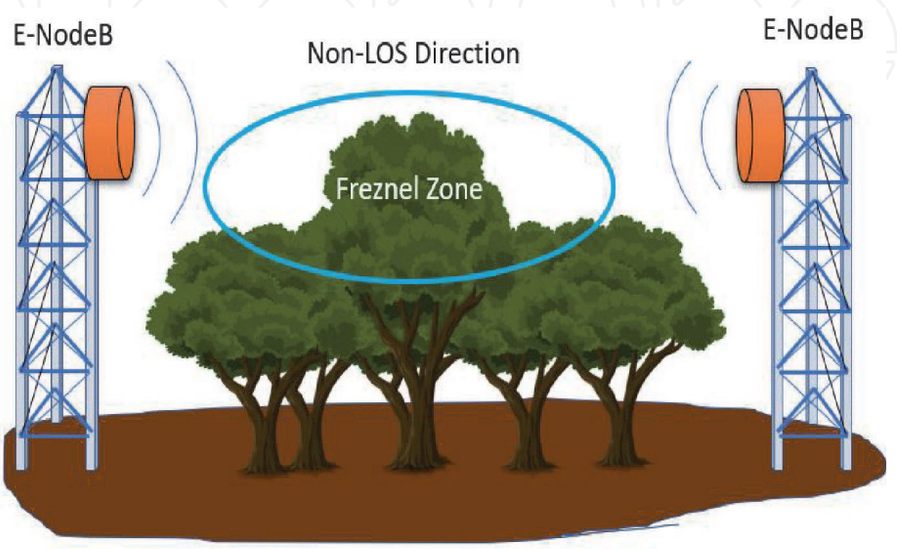

Figure 1.
Illustration of non line-of-sight (NLOS) propagation.

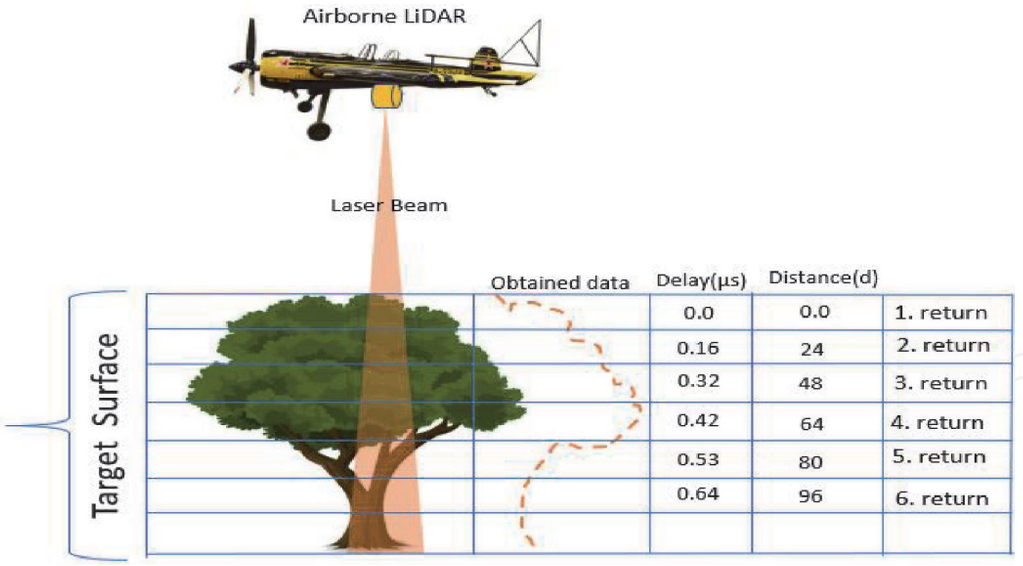

Figure 2.
Obtaining 3D point cloud using airborne LiDAR.

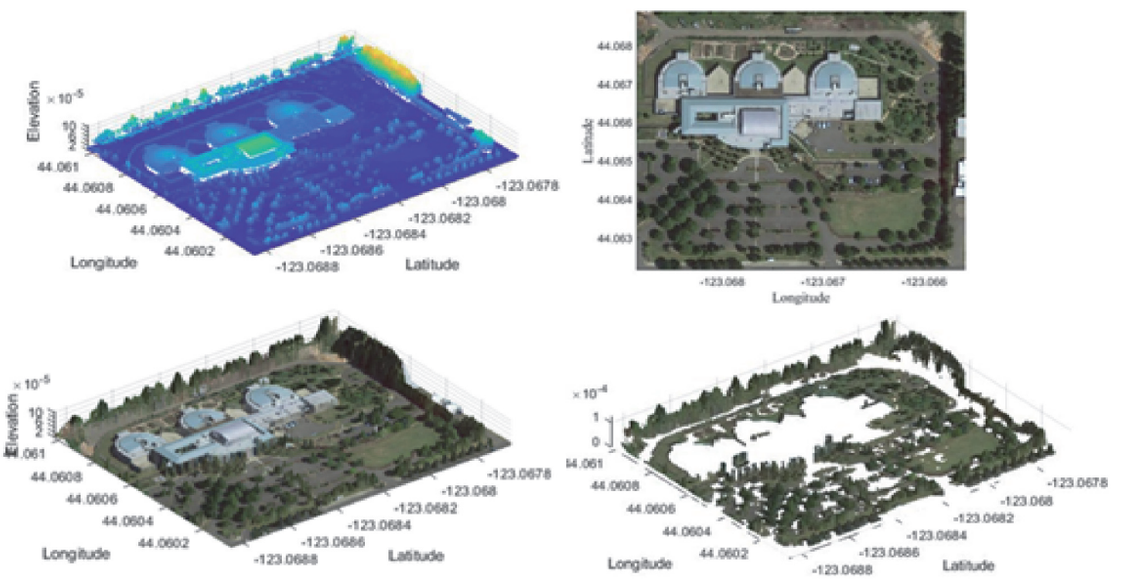

Figure 3.
3D Point cloud vegetation classification process.

Machine learning determines the learning patterns and builds a general decision algorithm by training some portion of data and is one of the most important parameters of smart cities. In this research, Artificial Neural Network (ANN) which is one of the most widely used machine learning algorithms will be used to build an adaptive SSPL model by using features obtained from 3D virtual environment. ANN consists of an input layer, hidden layer, and output layer [10]. A simplified illustration of an ANN is represented in **Figure 4**. A simple ANN with only one hidden unit is shown in **Figure 4**. In the input layer, the data $(x_1, x_2, .., x_n)$ and randomly initiated weights $(\theta_1, \theta_2, .., \theta_n)$ are multiplied and transmitted to the hidden layer, also known as the activation layer. In the hidden layer, a bias unit is added to the sum of the processed data, and the result goes through an activation function. A non-linear sigmoid function is usually used as an activation function and assigns 1 or 0 based on a threshold. In the next step, a gradient descent algorithm is used to adjust the connection weights between neurons. Gradient descent calculates errors between predicted and real values and finds the neuron

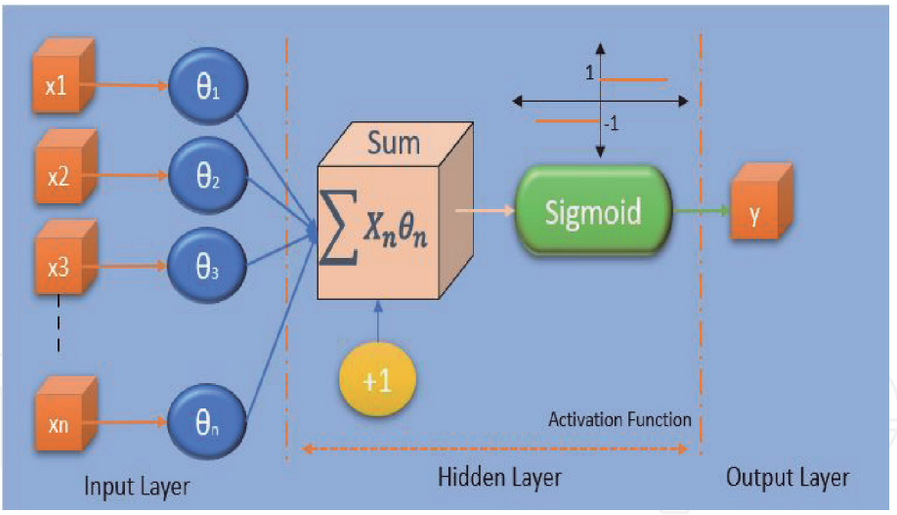

Figure 4.
Simple Presentation of a Perceptron.

weights that minimize the error by iteratively taking the gradients. This section will include an example using ANN with multiple hidden layers to estimate the SSPL of tree canopies. In this study, a powerful SSPL model has been created by using LiDAR and machine learning to solve MCS's aforementioned problems. The proposed model, having a combination of ANN and 3D point cloud, applies to large- and small-scale applications.

2. Related work

Many comprehensive studies have been conducted on Wireless Sensor Networks due to the continuous growth of mobile communication in smart cities. The studies mostly focus on power consumption and system accuracy [11]. In each study, different environments were tested over various aspects with image classification. However, image classification usage is not limited to a specific area but can be seen in almost all areas of studies. Juheon et al. performed an extensive study on the classification of individual tree species with LiDAR and deep learning [12]. Similarly, Torabzadeh et al. also studied tree species classification in forests with a combination of spectroscopy and airborne LiDAR [13] while Hartling et al. focused on urban tree species recognition and classification [14]. Image classification is a complex technique that finds space in many research areas. Image processing plays a crucial role in path loss analysis. In his study, Thrane aims to find the impact of buildings and multi-path propagation path loss of predefined signals [15]. He collects the signal attenuation measurements between the transmitter and receiver located in many different positions. After a 2D satellite image of the measurement area is obtained via Google Maps and rotated versions of images are prepared, the path loss effects of buildings are estimated with image classification and deep learning techniques. He states that 1 dB to 4.7 dB improvement factor in path loss prediction with his path loss model compared to empirical models. Likewise, the research conducted by Ahmadien et al. demonstrates a path loss model with K-mean clustering, deep learning techniques, and 3D images that converted from 2D satellite images via various simulation software [16]. Although 2D images are insufficient to create 3D images in many cases, he proposed a simulation-based path loss model in his study with limited parameters. Gracchi et al. uses a 3D point cloud taken by LiDAR to optimize WSN installation. High-resolution 3D point cloud data is analyzed to find a clear line of sight. She has validated her simulated 3D version of

the model with the LiDAR-based 3D point cloud visualization [17]. The next section will provide 3D image segmentation using geo-referenced satellite images.

3. Visualization of Trees Using Image Classification and 3D point Cloud

3.1 Direct geo-referencing and multi-sensor fusion

Direct geo-referencing is a highly efficient and accurate technique used to determine the location and direction of a Geo-MMS. Measurements of external orientation parameters such as altitude, orientation angles, and distances are used in geo-referencing. A cameraless illustration of the Geo-MMS system is shown in **Figure 5**.

Downward directed LiDAR under the plane takes rotational scans while IMU and GPS take separate measurements. The direct geo-referencing of a ground vector on the surface is computed by Eq. (1) [18].

$$\vec{X}_k^a = \vec{X}_b^a + R_b^a \left[R_L^b R_k^L \vec{x}_k^L + \Delta \vec{x}_b^L \right]; \tag{1}$$

Where: $\vec{X}_k^a$: The ground vector (a^{th} frame), R_L^a and R_L^b: Rotation matrix and boresight rotation, $R_k^L(\theta, \eta)$: The LiDAR mirror rotation, $\vec{x}_k^L$ and $\Delta \vec{x}_b^L$: Slant range of the LiDAR and boresight-shifts. The $R_k^L(\theta, \eta)$ is the function of the angle (θ) between ground and target. The angle (η) between ground and laser's X direction is calculated as follows.

$$R_k^L(\theta, \eta) = \begin{bmatrix} \cos\theta & -\sin\theta\sin\eta & -\sin\theta cos\eta \\ 0 & \cos\eta & -\sin\eta \\ \sin\theta & -\cos\theta\sin\eta & \cos\theta\sin\eta \end{bmatrix} \tag{2}$$

Kalman filter supported Inertial Navigation System (INS) geo-locates the data received by LiDAR and IMU by GPS data. A sequential adjustment is required since

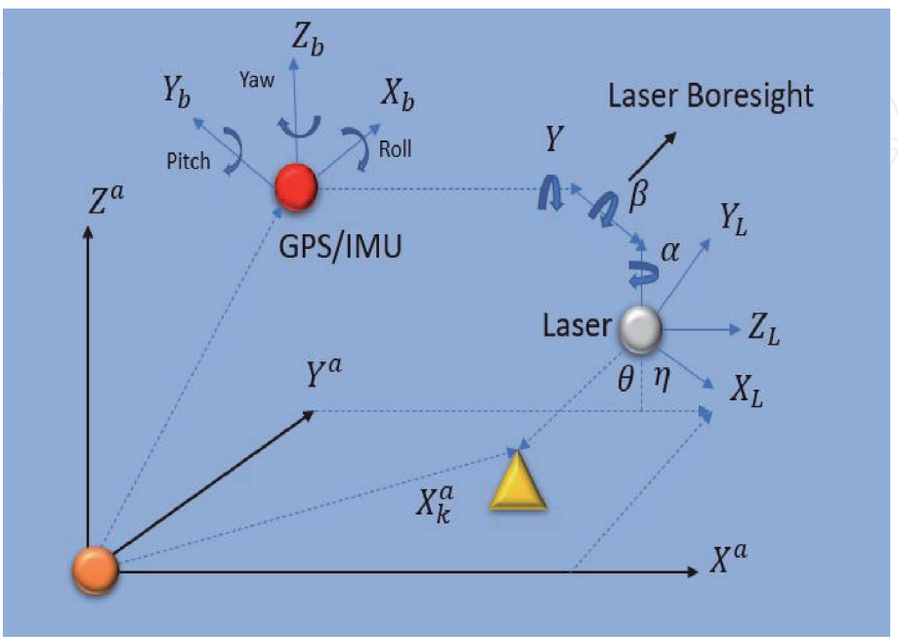

Figure 5.
Obtaining 3D point cloud using airborne LiDAR.

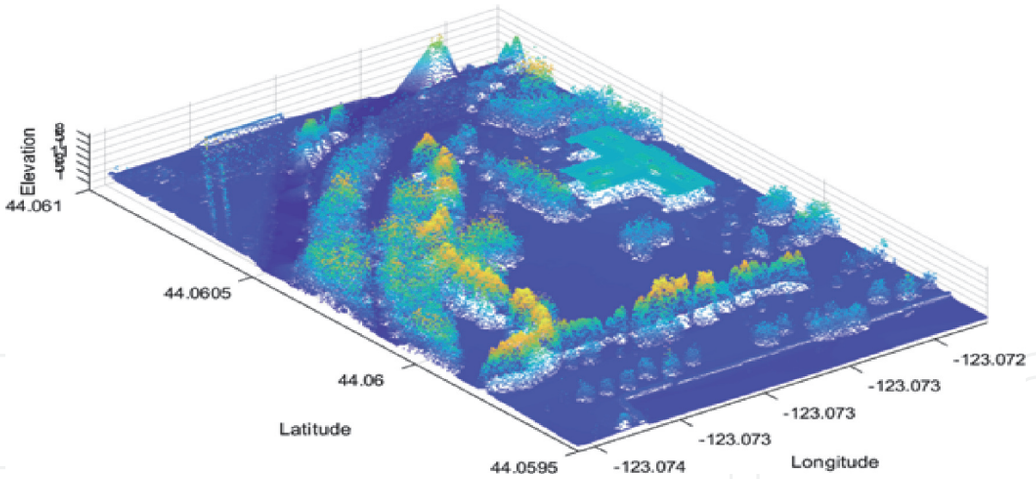

Figure 6.
2D satellite image of Florida Tech neighborhood.

each sensor operates in different frequencies. After synchronization is ensured and direct geo-referencing is complete, geo-referenced IMU and LiDAR data points are combined to visualize a 3D point cloud. An example of a 3D point cloud that belongs to the Lane County Mental Health service neighborhood located in Oregon is illustrated in **Figure 6** [19]. The LiDAR used in this example is operating at 70 kHz scanning speed and 1 cm resolution. The data is interpolated to fill the unmeasured spots and minimize the measurement error via Natural Neighbor Interpolation (NNI) [20]. It is also seen that the LiDAR data is geo-referenced in the x and y direction as longitude and latitude, respectively.

The corresponding 2D satellite image is also required for 2D/3D image fusion. The Google Map is utilized to extract the required geo-referenced 2D satellite image as represented in **Figure 7**.

3.2 Color classification for visualization of trees

Image classification is implemented to visualize necessary and informative properties using various methods through image processing. In this section, we apply a color-based classification using density and LAB color space. The images in RGB format are converted into LAB images since they are not suitable for digital manipulation. The three channels of LAB color space L, a, and b must be evaluated separately. After this process, with the help of Eq. (3), the intended color on the image will be picked to create a binary mask that will provide the average color of each channel falling on the selected mask on the image [21].

$$\mu = \left(\frac{1}{m \times n}\sum(m,n)P_{mask}(m,n)\right) \times Ones_{m\times n} \tag{3}$$

Find :$\mu_{maskL}, \mu_{maska}, \mu_{maskb}$

Relevant masks such as $mumask$, mu_{maska} and mu_{maskb} will be computed for each channel. The next step is to find the difference (Δ) between the masks and the channel as indicated in Eq.(4).

$$\begin{aligned} \Delta L_{M\times N} &= L - \mu_{maskL} \\ , \Delta L_{M\times N} &= a - \mu_{maska} \\ , \Delta L_{M\times N} &= b - \mu_{maskb} \end{aligned} \tag{4}$$

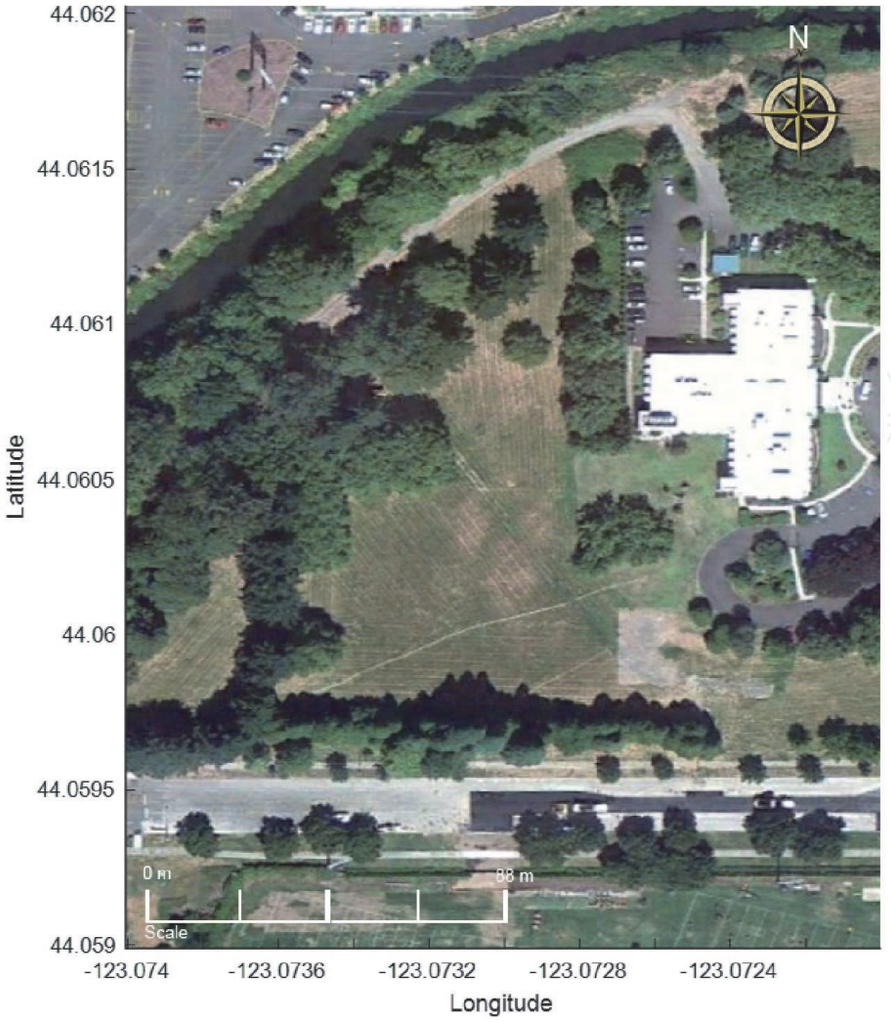

Figure 7.
2D satellite image of Lane County Mental Health service.

Since the masks alone represent only the drawn area, calculating the Euclidean distance for all three channels with the formula $\Delta E_{M\times N}$ will reveal the color values closest to the masked part of the image as seen in Eq. (5).

$$\Delta E_{M\times N} = \sqrt{(\Delta L)^2 + (\Delta a)^2 + (\Delta b)^2} \tag{5}$$

To obtain an efficient classification, the color estimation (ΔE_M) should fall in the 95% Confidence Interval (CI). This is essential since sharp color gradations within the area without tolerance can cause some areas to disappear. Thus, 95% CI should be applied to results by adding 3σ as seen in Eq.(6).

$$CI = \mu(\Delta E_{masked}) + 3\sigma(\Delta E_{Masked}) \tag{6}$$

Next, CI is applied to the ΔE to test $\Delta E <= CI$ values. If the condition is correct, logic one is assigned to this value. If not, logic 0 is assigned. The logical image containing zeros and ones is represented in **Figure 8a**. After implementing the logical image to the original image, the classified trees are obtained on a 2D satellite image. The classified image is demonstrated in **Figure 8b**. Since we aim to classify trees on the 3D point cloud, we can use that classified image to filter out undesired parts of the 3D point cloud other than trees, see **Figure 8c**. The results are shown in **Figure 9**.

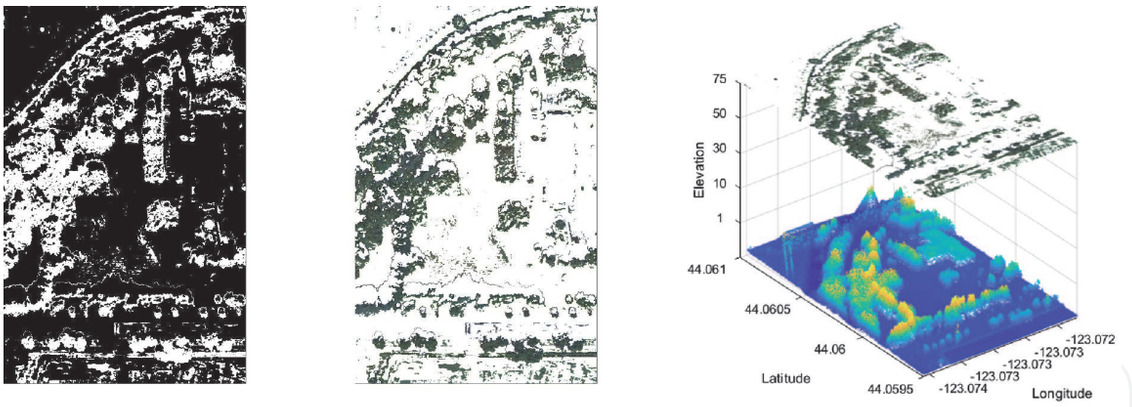

(a) Binary Filter (b) Classified Images (c) Filtering 3D image using 2D image.

Figure 8.
3D Filtering process of tree canopies.

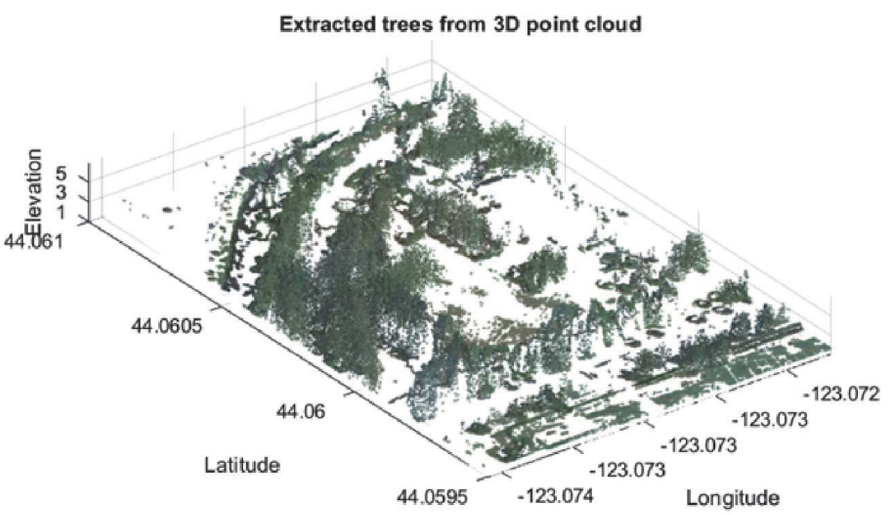

Figure 9.
Obtained extracted vegetation and trees from the environment.

4. Empirical models and proposed smart deployment technique

The signal's strength weakens when the signal encounters obstacles and loses energy due to multi-path reflection and absorption. The sum of the power loss and the signal path is called the signal strength path loss, which is decisive when deploying MCS. Therefore, many researchers have created path loss models such as Free-Space, Log-Normal, and Cost231-Hata models. Since each model emerges from experiments at a specific location, it has unique approaches specific to that location. In this research, we want to create a model supported by artificial intelligence and can fit in any location by getting out of location-oriented models that can be considered a disadvantage. All models, including the model to be obtained, were compared with each other. This model has been validated using the Mean Absolute Percent Error (MAPE).

4.1 Free-Space Path Loss Model

The free space path loss (FSPL) model determines the attenuation between the transmitter and the receiver in an unobstructed path. This phenomenon is indicated by the Friis transmission formula, as indicated in Eq.(7) [22].

$$FSPL = 10\log\left(\frac{P_t}{P_r}\right) = 10\log\left(\frac{(4\pi d)^2}{\lambda^2 G_t G_r}\right) \tag{7}$$

Where: λ: Wavelength, G_t: Gain of the transmitting antenna, G_r: Gain of the receiving antenna, d: Separation between transmitter and receiver.

4.2 Log-Normal Shadowing Path Loss Model

Log-normal shadowing (LNS) is the extended version of the Friis formula, which includes obstacles to the free space. It is a frequently used model for long-range propagation [23]. Because of the shadowing effect, the LNS model comprises Additive white Gaussian Noise (AWGN) represented as X_σ [24]. The LNS model is demonstrated in Eq. (8).

$$PL_{LNS}[dB] = PL(d_0) + 10\eta\log\left(\frac{d}{d_0}\right) + X_\sigma \tag{8}$$

Where: $PL(d_0)$: The path loss at d_0, η: Path loss exponent, X_σ: $N(0,\sigma)$ Normal distribution with zero mean. LNS model has the following environments and Path loss exponents, as shown in **Table 1**.

4.3 Cost231-Hata model

Cost 231-Hata model is an SSPL model that takes the Okumura Hata model to a more diverse frequency range (1500–2000 MHz). This model can be used mainly for urban, suburbans, and open areas. The Cost 231-Hata model is indicated in Eq. (9) [25].

$$\begin{aligned} PL_{C-231}[dB] = {} & 46.3 + 33.9\log(f) - 13.82\log(h_B) \\ & -a(h_R,f) + (44.9 - 6.55\log(h_B))\log(d) + C \\ \text{Where } a(h_R,f) = {} & (1.1\log(f) - 0.7)h_R - (1.56\log(f) - 0.8) \\ C = {} & \begin{cases} 0\,\text{dB for Suburban areas} \\ 3\,\text{dB for Urban areas} \end{cases} \end{aligned} \tag{9}$$

4.4 Proposed smart MCS deployment Technique

To design an intelligent broadcasting model for the deployment of MCS, the impact of vegetation must carefully be defined in the LOS direction. Towards LOS, the signal will be attenuated by transmission across vegetation due to reflections and absorption. Therefore, trees are measured as a highly complex obstruction in the environment from a telecommunication perspective. This phenomenon is expressed in **Figure 10**.

Environment	Path Loss Exponent (η)
Free Space	2
Urban area(Shadowed)	3–5
Inside building(LOS)	1.6–1.8

Table 1.
Predefined Path loss exponent (η) for different environments.

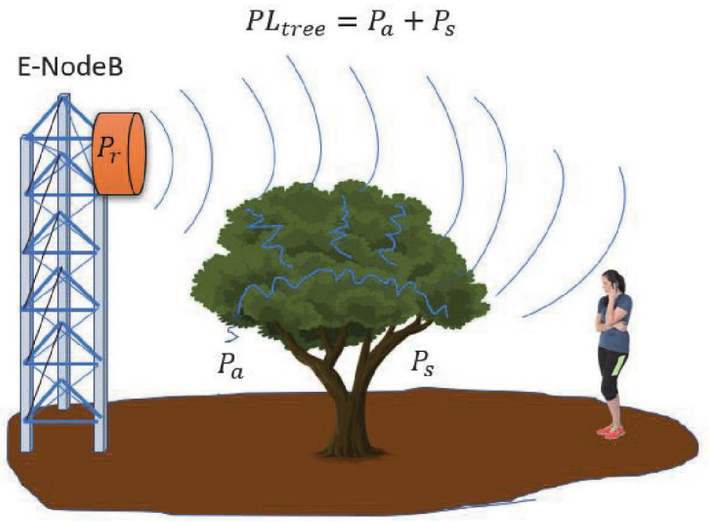

Figure 10.
Illustration of tree canopy path loss system.

This model is based on signal loss occurring on tree canopies (PL_{tree}) through scattering and absorption. In addition, considering P_a and P_s as the tree loss factor PL_{tree}, the corresponding signal strength loss is calculated as follows [26].

$$SSPL_{tree} = FSPL + PL_{tree} \tag{10}$$

In the literature, analysis of tree SSPL is a challenging ongoing research question. Even though the research numbers are going up, there are still a few consistent results due to the complex structure of the surveying area. This section extracts the features by means of image color classification and uses those features to reveal the required tree canopy path loss and add its effect to the FSPL through the ML algorithm. Since absorption and scattering are positively associated with the tree canopy's height and width, our algorithm will use these properties and estimate the required signal strength path losses.

4.4.1 Experiment and Model Presentation of Tree Canopy Path loss: case study

In this section, a experiment conducted by Egi et al. [18]. will be evaluated. From his study, the necessary training data were collected using a 40 m Mini Handheld Digital Laser Range Finder, LG G5 mobile phone. The application used for this experiment is a network activity application called Network Cell Info (by Wilysis). The phone is fixed in the LOS direction of the transmitter. To calculate PL_{tree}, the data is taken from the front and back sides of the tree canopy and subtracted from each other. This difference corresponds to the PL_{tree} caused by the scattering and absorption. This procedure is replicated in various places for different sizes of tree canopies. Since the data obtained are raw, feature normalization is applied to cause the gradient descent to converge faster. Mathematically explained, normalization is to subtract each feature's mean value from each item of the corresponding feature and scale the feature according to its standard deviation. Normalized data are used as input in our proposed model, as seen in **Figure 11**.

In this part, $x_1(height)$ and $x_2(width)$ are normalized and fed to the ANN. As the data pass through the perceptrons, they are multiplied by randomly initialized coefficients, called weights, (θ^j). At each layer, bias units (+1) are added to the data, which contribute to ANN's outcome by modifying the activation functions [27]. The parameters x_1, x_2 and, +1 with 200 elements are the input layers. The second layer is

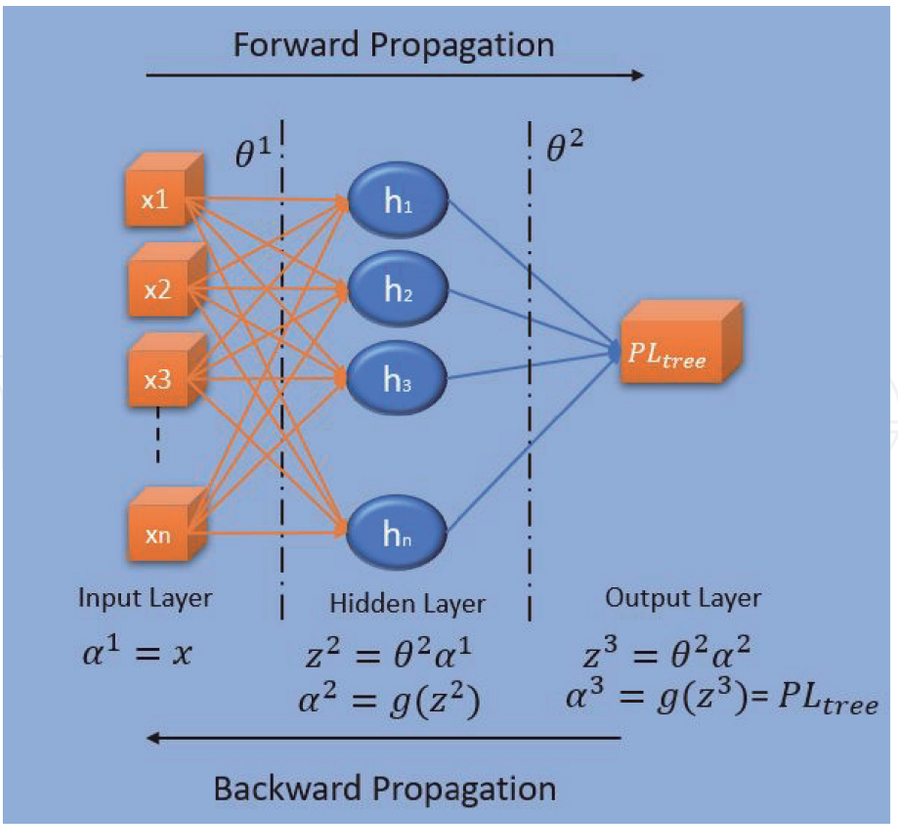

Figure 11.
Proposed ANN presentation.

the hidden layer consisting of 30 hidden units. The third layer is the output layer, which makes decisions based on the height and width taken from trees.

4.4.2 Calculating Cost Function Using Forward-propagation

In ANN, the data travels from the input layer to the output layer to make predictions. Since the propagation is only one direction towards forward, it is called forward-propagation. The data are exposed to weights and non-linear sigmoid functions throughout propagation to add non-linearity into the estimation model. A regularization parameter can also be used to increase the prediction accuracy [27]. After the prediction through forward-propagation, the cost is computed to measure the performance of the ANN model. The cost is calculated by cost the function which determines the error between real and predicted values. The cost function may differ based on the purpose of ANN. In this chapter, we use the logistic regression cost function, as seen in Eq. (11).

$$J(\theta) = \frac{1}{m}\sum_{i=1}^{m}\sum_{k=1}^{K=3}\left[-y_k^{(i)}\log\left(\left(PL_{tree}\left(x^{(i)}\right)\right)_k\right) - \left(1-y_k^{(i)}\right)\log\left(1-\left(PL_{tree}(x)^{(i)}\right)_k\right)\right] + \frac{\lambda}{2m}\left[\sum_{j=1}^{30}\sum_{k=1}^{2}\left(\theta_{j,k}^{(1)}\right)^2 + \sum_{j=1}^{3}\sum_{k=1}^{30}\left(\theta_{j,k}^{(1)}\right)^2\right] \tag{11}$$

where: $PL_{tree}\left(x^{(i)}\right)$ is the last activation function, K and m are the number possible outcomes and number of labels respectively, y is the observed outcome, θ's are the weights and λ is regularization parameter. The regulation parameter, λ, is

used to prevent over-fitting [26]. Random initial weights are required to break the symmetry and to utilize each hidden unit. Initial weights should be given in the $[-\varepsilon_{init}, \varepsilon_{init}]$ range to keep the parameters small and increase the learning efficiency. The formula for the required ε_{init} is given in Eq. (12).

$$\varepsilon_{init} = \frac{\sqrt{6}}{\sqrt{L_{in} + L_{out}}} \tag{12}$$

Where: L_{in} *and* L_{out} are number of units in adjacent layers. After forward-propagation process with $\lambda = 0.01$, the cost, J, is found as 2.052.

4.4.3 Back-propagation

Unlike forward-propagation, the back propagation propagates backward from the output layer to the input layer. While doing that, back-propagation computes gradients $(g'(z)^l)$ in every step towards backward. Gradient reveals (δ_j) changes in hidden layers. The subscript J indicates the number of iterations and changes regularly with each iteration in the back-propagation algorithm. This process is used for the optimization of the cost function. The sigmoid gradient is defined as follows:

$$sigmoid(z) = g(z) = \frac{1}{1 + e^{-z}} \tag{13}$$

$$g'(z) = \frac{d}{dz} g(z) = g(z)(1 - g(z)) \tag{14}$$

In the model, $(delta)$ errors given in Eq. (15) cause deviation and must be calculated in every layer [26].

$$\begin{aligned} \delta_j^{(3)} = \alpha_j^{(3)} - y_i \rightarrow \quad & Output \quad layer \\ \delta_j^{(2)} = \left(\theta^2\right)^T \delta^{(3)} .* g'\left(z^2\right) \rightarrow \quad & Hidden \\ \Delta^l = \Delta^l + \delta^{(l+1)} \left(\alpha^{(l)}\right)^T \rightarrow \quad & Adding \end{aligned} \tag{15}$$

The outcome of Δ^l is an unregularized gradient of the ANN cost function, which should be divided by m (total number of samples). During the process, it updates the θ value for all j's simultaneously. After training the data with a hundred forward and back-propagation, the cost was reduced from 2.052 to 0.636, resulting in an accuracy of 94.5% in signal strength estimation. Since the predicted accuracy is reached with our ANN algorithm, we apply our algorithm in the direction of LOS to the detected trees. Tree canopies are detected through the Local Maximum Method (LMM) and median filter processes.

4.4.4 Implementation of Local Maximum Method for detection of tree canopies

In order to determine the required parameter, the local maximums in the 3D point cloud must be calculated with some hypothetical constraints such as using 3×3 Median Filter, setting tree heights, width and peak to peak distance greater or equal to 1.6 m, 2 m, and 2 m, respectively. This will maximize the accuracy of the model by avoiding many deceptive local maxima. Local maxima are calculated using the following Eq. (16).

$$if\ \ f(x,y) > f\left(x_{nn}, y_{nn}\right) \tag{16}$$

Where: $f(x,y)$ is a pixel of an image, $f\left(x_{nn}, y_{nn}\right)$ are the neighborhood pixels of the f(x,y). By completing the training of the ANN, $LOS(SSPL_{tree}$ formula is obtained for LOS direction:

$$LOS(SSPL_{tree}[dB]) = FSPL[dB] + \sum_{j=0}^{n_{tree}} \left(\vec{PL}_{tree_j}\left(h_j, w_j\right)\right) \tag{17}$$

Where: $\vec{PL}_{tree_j}$: Predicted tree path loss, h_j: Height of the detected tree canopy, w_j: Width of the detected tree canopy.

4.4.5 Model Validation with MAPE

Mean Absolute Percent Error (MAPE) is a statistical method to measure the prediction accuracy of models. MAPE determines the differences between real and theoretical values. Later it divides this difference by the real values. Next, the absolute values of the results are averaged and represented as a percentage. MAPE is determined by Eq. (18) [28].

$$LOS(MAPE[\%]) = \frac{100\%}{n} \sum_{i=1}^{n} \left| \frac{Models - PL_{real}}{PL_{real}} \right| \tag{18}$$

5. Analysis and results of a case study

This study is based on a comparison of four models, including PL_{tree}. The 3D environment obtained by airborne LiDAR belongs to the Florida Institute of Technology neighborhood. Since the data has some faulty values, the natural neighbor interpolation is performed on the raw 3D point cloud. To create a colorful 3D image, the geo-referenced 2D satellite image is imported via Google API and merged with the 3D point cloud. Later, the tree canopies are located by the local maxima method on a 2D image. This 2D classified image helped us extract and locate trees on the 3D point cloud. The process of extracting tree canopies from the 3D point cloud is shown in **Figure 12**.

While the detected trees are marked with red ×, the labeled transmitter and receiver belonging to MCS are marked with yellow + signs. Using the LMM technique and limitations, the height and width of five trees were plotted. The proposed ANN algorithm will be used to estimate the required PL_{tree} value for each tree canopy detected in the LOS direction, where the characteristics of the environment such as height and width are obtained. The properties of five trees, such as distance, width, height, and PL_{tree} are shown in **Table 2**. It is seen from **Table 2**, there is a correlation between tree size and estimated PL_{tree}. This is because the complex structure of the tree canopies causes more reflection and absorption in proportion to the tree's size. The detected features from the environment are used as input data for the ANN model, and compared with the other empirical models with the same parameters. The results are listed in **Table 3**. It is seen that the energy demand of LNPL and Cost231 models increased with the distance exponentially, but they could not provide the required signal power considering the real values. This is because traditional propagation models assume that terrains have the same characteristics when it comes to terrain pattern. For this reason, they deviate significantly in terms

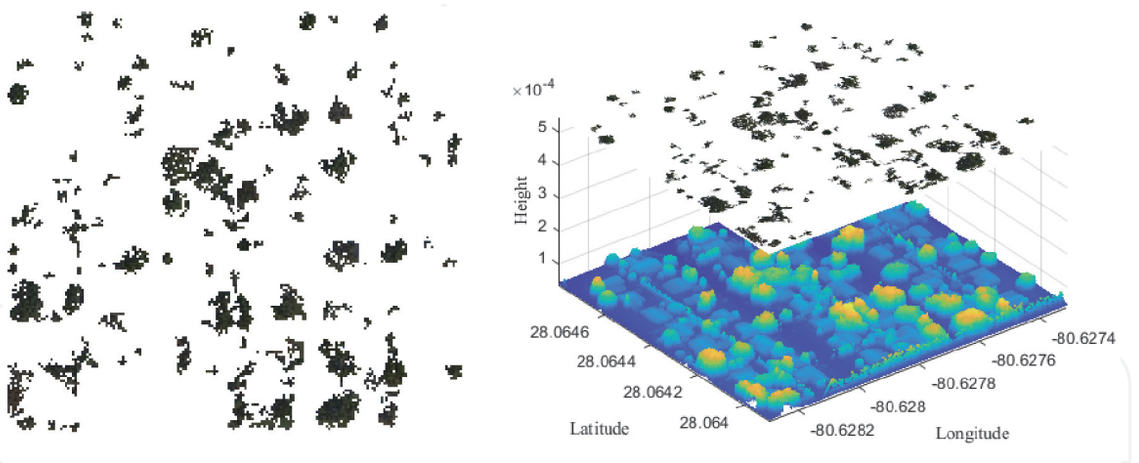

(a) Classified Image (b) Filtering 3D image using 2D image.

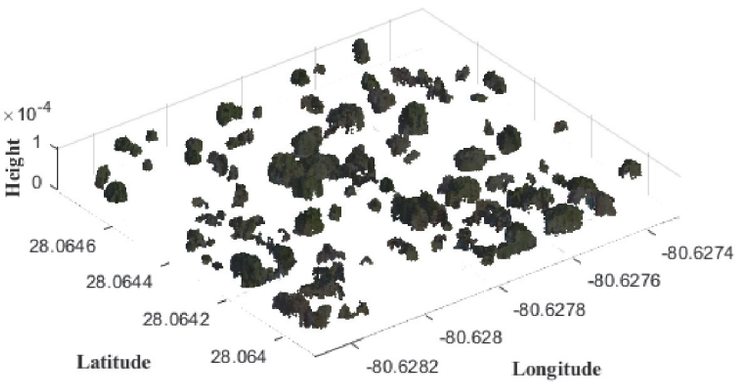

(c) Filtered tree canopies

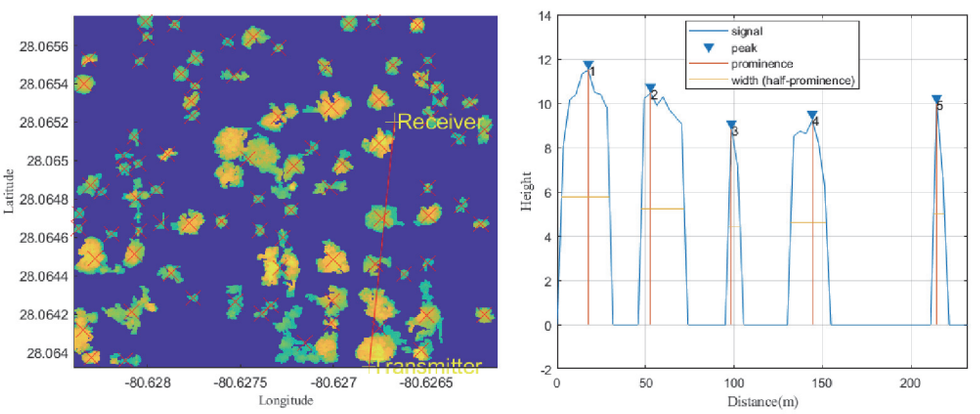

(d) The heat map of 3D extracted tree canopies and Tx and Rx locations. (e) The detected tree canopies and their locations.

Figure 12.
3D Filtering process of tree canopies.

of SSPL and RSL estimations. The performance of $SSPL_{tree}$ is also shown in **Figure 13**. According to **Figure 13**, All models have a strong relationship in terms of distance and SSPL. However, unlike other models, the tree SPPL is discerning itself by showing a peak anytime propagation encounter a tree in the LOS direction. To see whether the model is performed well or not, RSL measurement should be compared with real values. In this case study, RSL values are taken through transmitter and receiver facing each other with an operating frequency of 2110 MHz. The devices have effective radiated power of -1 dB. All empirical models and SSPL tree predicts the RSL results operating with these parameters. The results are

Distance(m)	n_{tree}	**Height**(m)	**Width**(m)	PL_{tree}**[dB]**
17	1	11.4	13.05	3 dB
52	2	10.45	12.15	3 dB
98	3	8.8	3.31	1 dB
144	4	9.2	10.5	3 dB
214	5	9.9	3.15	1 dB

Table 2.
Detected features and obtained PL_{tree}.

Distance(m)	n_{tree}	$\text{SSPL}_{\text{tree}}$**[dB]**	**FSPL[dB]**	**LNPL[dB]**	**Cost231[dB]**
17	1	49.4	46.41	48.14	30.04
52	2	60.93	54.93	58.26	45.05
98	3	67.1	60.1	64.4	54.14
144	4	73.3	63.32	68.22	59.81
214	5	77.7	66.7	72.24	65.72

Table 3.
Comparison of Tree Canopy Path loss with empirical models.

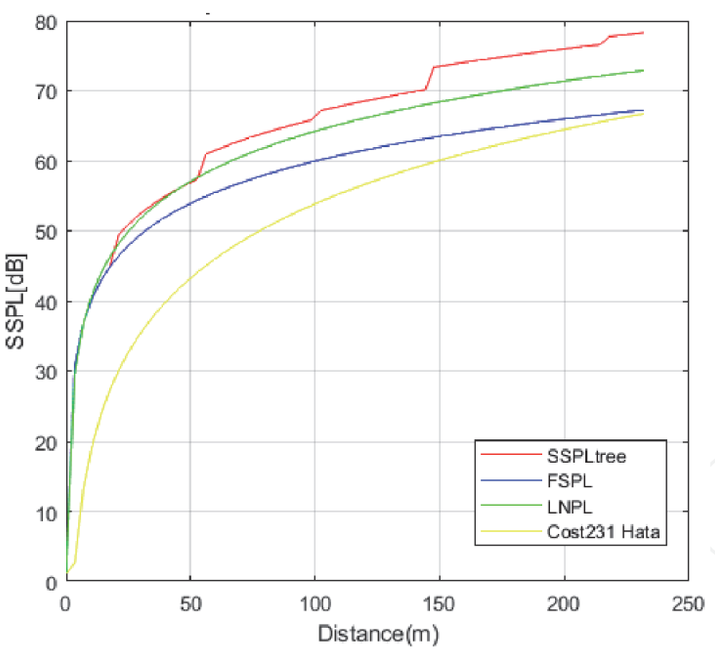

Figure 13.
Comparison of 4 Models with respect to distance.

presented in **Figure 14**. The RSL values are significant in terms of maintaining the communication between transmitter and receiver. That is why it is essential to keep the predicted values as close as the real values. In **Figure 14**, it is indicated that the red line, which is tree RSL (RSL_{tree}), has a similar track with the black line, which is measurement RSL($mRSL$). This proves that the ANN aided model has over-performed among all empirical models. MAPE results also validate these results. From **Table 4**, RSL_{tree} have a minimum deviation of 4.26% in terms of MAPE percentage while others result stayed in between 6.29% to 16.9%.

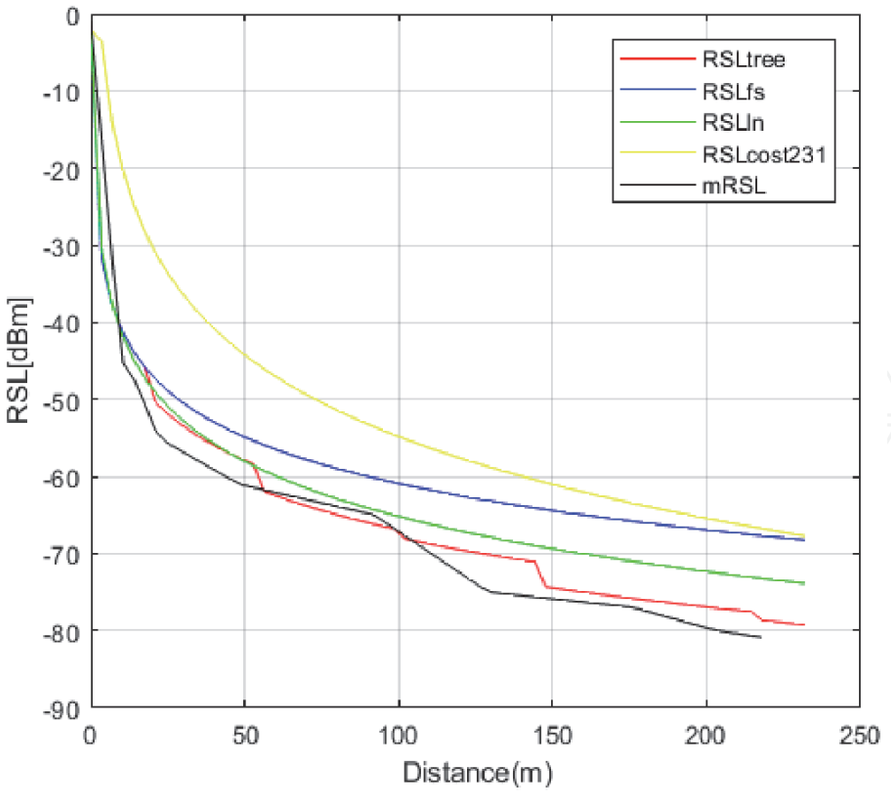

Figure 14.
RSL Comparison of Models and Measured values with respect to distance.

	n_{tree}	RSL_{tree}	RSL_{fs}	RSLln	RSLCost231
MAPE%	5	4.26	10.16	6.29	16.9

Table 4.
The MAPE performance of the models.

AI aided RSL tree model with the a deviation of 4.26% has a significant improvement compared to other empirical models since all the micro-variations contribute to the estimates. In addition, unpredictability of tree variations [29] was overcome using artificial intelligence. The proposed model result was also outperformed compare to A. Alsayyari et al. case study with MAPE results of % 34.37 and %19.80 [30].

6. Conclusions

This chapter demonstrated the fusion of state of art technologies that can potentially contribute to developing an intelligent environment for smarter cities. Sensor fusion, UAV, satellite image, and image classification have integrated for the purpose of creating a 3D virtual environment for a realistic data platform. The obtained information is crucial in terms of the evaluation of the planned projects for futuristic cities. In our case, we have assessed the effect of trees upon smart deployment of MCS using 3D point cloud, which is basically the 3D virtual presentation of the city, to maintain connectivity and efficiency. Since tree canopies are considered irregular terrains and their complex structure highly affect the efficiency of SSPL due to multi-path reflection, we extracted tree canopies by using 2D color classified satellite image as a filter. By means of extracted 3D point cloud

information of tree canopies, the features (height and width) are obtained for the purpose of training the ANN. The data and results that are taken from Egi et al.'s case study are a good demonstration of the model application. The analysis shows that the created smart model can significantly affect the MCS' propagation since it adds all micro-variations and utilizes tree features for adjustment of RSL. The MAPE results for all models are obtained as 4.26%, 10.16%, 6.29%, and 16.9% error for PL_{tree}, FSPL model, log-normal model, and the Cost 231-Hata model, respectively. It should also be pointed out that the ANN model did not consider the effect of the buildings. This effect may be added to the model in future applications. The primary contribution of this chapter is to create a colorful 3D virtual environment and make more precise feature extraction possible. This technique may also shape the future of smart cities by using digitized information for city planning, communication planning, and infrastructure planning. It should be noted that the proposed model is only applicable to outdoor applications since the 3D virtual environment only provides outdoor information. This limitation can be also removed if the LiDAR scanning is performed indoors and combined with the outdoor data.

Author details

Yunus Egi[1,2*†] and Engin Eyceyurt[2†]

1 Sirnak University, Sirnak, Turkey

2 Florida Institute of Technology, Melbourne, FL, USA

*Address all correspondence to: yunusegi@sirnak.edu.tr

† These authors contributed equally.

References

[1] Shirowzhan S, Tan W, Sepasgozar SME. Digital Twin and CyberGIS for Improving Connectivity and Measuring the Impact of Infrastructure Construction Planning in Smart Cities. ISPRS Int. J. Geo-Inf. 2020; **9**:240. DOI: https://doi.org/10.3390/ijgi9040240

[2] Stoll C. Michael Arthur Mehling, COVID-19: Clinching the Climate Opportunity. One Earth. 2020;**3**(4): 400-404, ISSN 2590-3322. DOI: https://doi.org/10.1016/j.oneear.2020.09.003

[3] Qi Q, Tao F, Hu T, Anwer N, Liu A. Yongli Wei. A.Y.C. Nee, Enabling technologies and tools for digital twin, Journal of Manufacturing Systems: Lihui Wang; 2019 ISSN 0278-6125

[4] Shanker Y, Lobiyal DK. Role of earth bulge on the prediction of radio propagation path loss over irregular terrain. International Journal of Wireless and Mobile Computing. 2020; **18**(4):352-360

[5] Carpenter, John, et al. Investigations and analyses of LTE network cell tower deployments and impact on path loss calculations. MITRE CORP BEDFORD MA BEDFORD United States, 2019.

[6] Mir Ghoraishi, Jun-ichi Takada, Tetsuro Imai,"Radio Wave Propagation Through Vegetation" 17 01 2019. [online].Available:http://cdn.intechopen.com/pdfs/42732/InTech-Radiowave propagationthroughvegetation.pdf.

[7] Ribero, MÃ³nica, et al. "Deep learning propagation models over irregular terrain." ICASSP 2019–2019 IEEE International Conference on Acoustics, Speech and Signal Processing (ICASSP). IEEE, 2019.

[8] Getis A. Introduction to Geography: Earth sciences. CTI Reviews: Physical geography; 2016

[9] Cramer M et al. ULTRA-HIGH PRECISION UAV-BASED LIDAR AND DENSE IMAGE MATCHING. Remote Sensing Spatial Information Sciences: International Archives of the Photogrammetry; 2018

[10] Rodrigo Fernandes de Mello; Moacir Antonelli Ponti, Machine Learning"A practical approach on statistical Learning Theory", Sao Paulo: Springer, 2018.

[11] Sherazi, Hafiz Husnain Raza, Luigi Alfredo Grieco, and Gennaro Boggia. "A comprehensive review on energy harvesting MAC protocols in WSNs: Challenges and tradeoffs." Ad Hoc Networks 71 (2018): 117–134.

[12] Juheon, et al. Individual tree species classification from airborne multisensor imagery using robust PCA. IEEE Journal of Selected Topics in Applied Earth Observations and Remote Sensing. 2016;**9**(6):2554-2567

[13] Torabzadeh, Hossein, et al. "Tree species classification in a temperate mixed forest using a combination of imaging spectroscopy and airborne laser scanning." Agricultural and Forest Meteorology 279 (2019): 107744.

[14] Hartling, Sean, et al. "Urban tree species classification using a WorldView-2/3 and LiDAR data fusion approach and deep learning." Sensors 19.6 (2019): 1284. org/citation.cfm?doid=1711113.1711127. [Accessed 6 1 2018].

[15] Thrane J, Zibar D, Christiansen HL. Model-aided deep learning method for path loss prediction in mobile communication systems at 2.6 GHz. Ieee Access. 2020;**8**:7925-7936

[16] Ahmadien O et al. Predicting Path Loss Distribution of an Area from Satellite Images Using Deep Learning. IEEE Access. 2020;**8**:64982-64991

[17] Gracchi, Teresa, et al. "Optimizing Wireless Sensor Network Installations by Visibility Analysis on 3D Point Clouds." ISPRS International Journal of Geo-Information 8.10 (2019): 460.

[18] Egi Y, Otero CE. Machine-Learning and 3D Point-Cloud Based Signal Power Path Loss Model for the Deployment of Wireless Communication Systems. IEEE Access. 2019;**7**:42507-42517

[19] F. I. University, "International Hurricane Research Center," 12 12 2018. [Online]. Available:http://dpanther2.ad.fiu.edu /Lidar/lidarNew.php.

[20] Liu P et al. Fusion of color histogram and LBP-based features for texture image retrieval and classification. Information Sciences. 2017;**390**:95-111

[21] MATLAB, "Segmentation methods in image processing and analysis," MATLAB, 18 June 2018. [Online]. Available:https://www.mathworks.com/

[22] Breinbjerg, Olav, and Kyriakos Kaslis. "On the accuracy of Friis' transmission formula at short range." 2017 XXXIInd General Assembly and Scientific Symposium of the International Union of Radio Science (URSI GASS). IEEE, 2017.

[23] MacCartney, George R., and Theodore S. Rappaport. "Study on 3GPP rural macrocell path loss models for millimeter wave wireless communications." 2017 IEEE International Conference on Communications (ICC). IEEE, 2017.

[24] Silvia Demetri ; Gian Pietro Picco ; Lorenzo Bruzzone, "Estimating Low-power Radio Signal Attenuation in Forests: A LiDAR-based Approach," in Distributed Computing in Sensor Systems (DCOSS), 2015 International Conference on, Cambridge, 2015.

[25] Braga, Allan Dos S., et al. Radio Propagation Models Based on Machine Learning Using Geometric Parameters for a Mixed City-River Path. IEEE Access. 2020;**8**:146395-146407

[26] de Jong YLC, Herben MHAJ. A tree-scattering model for improved propagation prediction in urban microcells. in IEEE Transactions on Vehicular Technology. March 2004; **53**(2):503-513. DOI: 10.1109/TVT.2004.823493

[27] A. Ng, "Machine Learning lecture 4," 14 01 2019. [Online]. Available: https://www.coursera.org/learn/machine-learning.

[28] Olasupo TO, Otero CE, Olasupo KO, Kostanic I. Empirical Path Loss Models for Wireless Sensor Network Deployments in Short and Tall Natural Grass Environments. in IEEE Transactions on Antennas and Propagation. Sept. 2016;**64**(9): 4012-4021

[29] de Jong YLC, Herben MHAJ. A tree-scattering model for improved propagation prediction in urban microcells. in IEEE Transactions on Vehicular Technology. March 2004; **53**(2):503-513. DOI: 10.1109/TVT.2004.823493

[30] A. Alsayyari, I. Kostanic, C. E. Otero and A. Aldosary, "An empirical path loss model for wireless sensor network deployment in a dense tree environment," 2017 IEEE Sensors Applications Symposium (SAS), Glassboro, NJ, 2017, pp. 1–6, doi: 10.1109/SAS.2017.7894099.